

Substantial extension of the lifetime of the terrestrial biosphere

R.J. GRAHAM ¹, ITAY HALEVY ² AND DORIAN ABBOT ¹

¹*Department of Geophysical Sciences, University of Chicago
5734 S. Ellis Ave.*

Chicago, IL 60637, USA

²*Department of Earth and Planetary Sciences, Weizmann Institute of Science
234 Herzl St.
Rehovot, Israel*

ABSTRACT

Approximately one billion years (Gyr) in the future, as the Sun brightens, Earth’s carbonate-silicate cycle is expected to drive CO₂ below the minimum level required by vascular land plants, eliminating most macroscopic land life. Here, we couple global-mean models of temperature- and CO₂-dependent plant productivity for C₃ and C₄ plants, silicate weathering, and climate to re-examine the time remaining for terrestrial plants. If weathering is weakly temperature-dependent (as recent data suggest) and/or strongly CO₂-dependent, we find that the interplay between climate, productivity, and weathering causes the future luminosity-driven CO₂ decrease to slow and temporarily reverse, averting plant CO₂ starvation. This dramatically lengthens plant survival from 1 Gyr up to ~1.6-1.86 Gyr, until extreme temperatures halt photosynthesis, suggesting a revised kill mechanism for land plants and potential doubling of the future lifespan of Earth’s land macrobiota. An increased future lifespan for the complex biosphere may imply that Earth life had to achieve a smaller number of “hard steps” (unlikely evolutionary transitions) to produce intelligent life than previously estimated. These results also suggest that complex photosynthetic land life on Earth and exoplanets may be able to persist until the onset of the moist greenhouse transition.

1. INTRODUCTION

In the far future, as the Sun brightens, Earth’s surface will warm, and in response the carbonate-silicate cycle (Walker et al. 1981) is expected to draw CO₂ out of the atmosphere through climate-dependent silicate weathering and carbonate burial (Caldeira & Kasting 1992). This will create an increasingly stressful environment for land plants, eventually driving them extinct through CO₂ starvation, at the CO₂ compensation point, or through overheating, at their upper temperature threshold (Lovelock & Whitfield 1982; Caldeira & Kasting 1992). This would also lead to the extinction of macroscopic life on land that relies on land plants (Judson 2017). Most previous work has concluded that CO₂ starvation is the more likely kill mechanism and that this is likely to occur approximately 1 billion years (Gyr) in the future (Table 1).

The rate of silicate weathering at the planetary scale is usually assumed to vary exponentially with temperature, with an e-folding scale of T_e , and to have a power-law dependence on CO₂, with an exponent β (Eq. 1). Most previous work (Table 1) has assumed that silicate weathering is strongly temperature-dependent ($T_e \approx 10\text{--}20$ K) and weakly CO₂-dependent ($\beta \approx 0.25\text{--}0.5$). Recent studies instead support a much weaker effective temperature dependence, with $T_e = 30\text{--}40$ K (Maher & Chamberlain 2014; Krissansen-Totton & Catling 2017; Winnick & Maher 2018; Graham & Pierrehumbert 2020; Herbert et al. 2022; Brantley et al. 2023). The CO₂ dependence of silicate weathering has received less attention than the temperature dependence, but a range of $\beta = 0.2\text{--}0.9$ is allowed by available data (Krissansen-Totton & Catling 2017; Palandri & Kharaka 2004; Winnick & Maher 2018; Hakim et al. 2021).

Life’s expansion onto land likely increased the dissolution rate of silicate minerals at Earth’s surface under a given set of climate conditions, leading to lower equilibrium CO_2 and lower surface temperatures to maintain balance between weathering and outgassing (Volk 1987; Berner 1992; Schwartzman 2017). This biotic weathering enhancement results mostly from plant acidification (through organic acid excretion and increased belowground respiration) and stabilization of soils, as well as changes in water cycling (Berner 1992; Berner et al. 2003; Taylor et al. 2009, 2011; Ibarra et al. 2019; Dahl & Arens 2020). The degree to which vascular plants accelerate silicate weathering under a given set of climate conditions is debated, but experiments suggest a biotic weathering enhancement factor of ≈ 2 -10 (Moulton & Berner 1998; Moulton et al. 2000; Dahl & Arens 2020).

Lifespan [Gyr]	Kill mech.	T_e [K]	β	Ref.
0.1	CO_2	n/a	n/a	(Lovelock & Whitfield 1982) ^a
0.9	CO_2	13.7	0.25 ^b	(Caldeira & Kasting 1992)
0.5-0.8	CO_2	13.7	0.25 ^b	(Franck et al. 1999)
0.5	CO_2	13.7	0.25 ^b	(Franck et al. 2000)
0.8-1.2	T	13.7	0.25 ^b	(Lenton & von Bloh 2001) ^c
1.2	CO_2	13.7	0.25 ^b	(Franck et al. 2002)
0.5-1.2	T	13.7	0.25 ^b	(Von Bloh et al. 2003)
0.8-1.2	T	13.7	0.25 ^b	(Franck et al. 2006)
1.3	CO_2	13.7	0.3	(Rushby et al. 2018)
0.8	CO_2	10.9	0.5	(de Sousa Mello & Friaça 2020)
1.0-1.3	CO_2	8.0 - 22.2	0.5	(Ozaki & Reinhard 2021)
0.9	CO_2	17.2	0.5	(Mello & Friaça 2023) ^d
0.5-1.86	T	12-48	0.05-0.91	This work

Table 1. Estimates of the future lifespan of land plants. The first column lists estimates of the future lifespan of vascular land plants from previous work and this study. The second column lists each study’s preferred extinction mechanism for land plants: overheating (“ T ”) or CO_2 starvation (“ CO_2 ”). The third column lists e-folding temperatures for silicate weathering used in each study. The fourth column lists power-law CO_2 dependences of silicate weathering used in each study. The final column provides references. The bottom row (in bold) summarizes the results and weathering model parameters used in this study.

^a Lovelock & Whitfield (1982) assumed land plant extinction below $p\text{CO}_2 = 15$ Pa (150 ppmv) and did not utilize an explicit weathering model.

^b These β values come from converting a H^+ activity power-law (Caldeira & Kasting 1992), which has a 0.5 power, to the equivalent direct CO_2 power law, which reduces the power by a factor of two (Berner 1992).

^c Lenton & von Bloh (2001) included an additional “biotic enhancement factor” in their weathering model that results in somewhat different behavior from the weathering models in the other studies listed.

^d Mello & Friaça (2023) included a seafloor weathering component with an e-folding temperature of 9.9 K and a CO_2 power of 0.3.

In this study, we apply global-mean models of plant productivity, the carbon cycle, and climate to constrain the lifespan and eventual extinction mechanism of land plants and the species that rely on them (the complex biosphere). For the first time, we consider the weaker temperature dependence and potential for a stronger CO_2 dependence of silicate weathering suggested by recent data. We also separately model C_3 and C_4 plant productivity and their effect on silicate weathering. With these new constraints on silicate weathering, and barring technological intervention or extreme evolutionary adaptation, we find that the complex terrestrial biosphere will be exterminated thermally at temperature and insolation levels approaching moist or runaway greenhouse conditions (Leconte et al. 2013; Wolf & Toon 2014, 2015). This result emphasizes the importance of carbon cycle parameterization for predicting Earth’s far future and underscores the need for further validation with more sophisticated climate models. If life is common

beyond Earth, our conclusions may be testable with future observations of biosignatures on extrasolar planets. In the discussion we also touch on potential implications of a longer biosphere lifespan for the prevalence of life in the universe.

2. METHODS

2.1. Plant CO_2 and temperature limits

Most previous attempts to estimate the future lifespan of this component of the biosphere have assumed a minimum CO_2 for land plants (“ CO_2 compensation point”) of 10 parts per million by volume (ppmv) of CO_2 and a maximum growth temperature of 323 K (Caldeira & Kasting 1992; Franck et al. 1999, 2000; Lenton & von Bloh 2001; Franck et al. 2002; Von Bloh et al. 2003; Franck et al. 2006; Rushby et al. 2018; de Sousa Mello & Friaça 2020; Ozaki & Reinhard 2021; Mello & Friaça 2023). We argue that both of these choices are too conservative.

Land plant carbon fixation is driven by two main metabolisms known as C_3 and C_4 , responsible for $\approx 70\text{--}82\%$ and $\approx 18\text{--}30\%$ of plant productivity respectively (François et al. 1998; Raven et al. 2008; Blunier et al. 2012). C_3 plants, lacking the mechanism C_4 plants use to concentrate CO_2 near the Rubisco proteins in their cells, have a relatively high CO_2 compensation point between approximately 30 and 100 ppmv CO_2 , depending on plant species and background temperature (under modern O_2 conditions) (Collatz et al. 1992; Nobel 2020). C_4 plants, due to their carbon concentrating mechanism (Raven et al. 2008; Edwards & Ogburn 2012), can survive down to much lower CO_2 levels of between ≈ 0 and 10 ppmv (Chen et al. 1970; Collatz et al. 1992; Nobel 2020). As described in section 2.4, our default parameter choices for the C_4 plant productivity model utilized in this study produce a CO_2 compensation point of 2.9 ppmv, which serves as the minimum CO_2 level required for plant growth in this study. This may be a conservative choice, since several plants are known to have CO_2 compensation points below this limit (Chen et al. 1970).

As noted before, the upper temperature limit for land plants in studies of the future lifespan of the complex terrestrial biosphere is frequently taken to be 323 K (50 C) (e.g. Caldeira & Kasting 1992). However, a number of plants living in desert and hydrothermal environments can survive and photosynthesize through periodic exposure to temperatures at and above this putative limit, and plant temperature optima tend to mirror the maximum temperatures encountered in their local environments (Prado et al. 2023). These factors suggest the range of observed thermal tolerances for plants may simply reflect the range of environments present on Earth today. As an example of a plant that pushes up against the 323 K boundary, field observations of the C_4 shrub *Hammada scoparia* in the Negev desert suggest a seasonal photosynthetic optimum temperature of 313 K (40 C), with photosynthesis remaining above zero up to a temperature of 333 K (60 C) (Lange et al. 1974). A few plants display photosynthetic temperature optima even higher than *H. scoparia* (Prado et al. 2023, Data S3). One of the most extreme known examples is the thermophilic C_4 desert perennial *Tidestromia oblongifolia*, which reaches a maximum photosynthesis rate at 320 K (47 C) (Björkman et al. 1972) and grows exponentially during Death Valley summers that regularly subject plants to temperatures of between 46 and 50 C (Prado et al. 2023). Although *T. oblongifolia*’s upper temperature limit for photosynthesis does not appear to have been recorded, its optimum temperature is 7 K higher than that of *H. scoparia*, suggesting it may be able to photosynthesize several degrees above *H. scoparia*’s 333 K limit. Extrapolation with a simple cubic spline fitted to observations from Prado et al. (2023) of *T. oblongifolia*’s photosynthesis rate between 306 K (33 C) and 323 K (50 C) suggests the species could potentially photosynthesize (likely with significant damage) up to 336 K (63 C) (see Fig. 1). Regardless of the exact value of its upper temperature limit, the fact that *T. oblongiformia* operates with near-peak photosynthetic rates at 323 K seems to invalidate that temperature as a fundamental threshold for plant growth.

The upper temperature limit for land plants can be estimated from the highest temperature they have been observed to survive (Clarke 2014). Although a thermal limit for eukaryotic organisms in general of 333 K is often cited (Tansey & Brock 1972), the temperature record for land plants appears to be held by *Dichantheium lanuginosum*, a C_3 grass growing in geothermal settings that can remain healthy through weeks of daily 10-hour-long exposures to rhizosphere temperatures of 338 K (when colonized by the fungus *Curvularia protuberata* while the fungus is infected with *Curvularia* thermal tolerance virus) (Brown & Smith 1975; Redman et al. 2002; Márquez et al. 2007; Clarke 2014). A similar degree of thermotolerance was conferred on tomato plants (Márquez et al. 2007), watermelons, and wheat (Pennisi 2003) that were inoculated with the virus-infected fungus, suggesting the mechanism mediating the effect in the grass may be generally applicable. At face value, the possibility of plant survival at 338 K seems implausible, in particular since enzymes necessary to maintain Rubisco activity have been found to rapidly denature and become

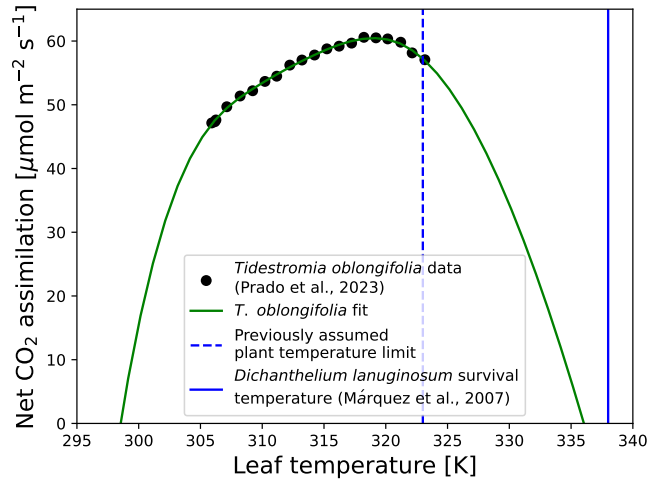


Figure 1. Comparing *Tidestromia oblongiformia* and *Dichantheium lanuginosum* temperature data to previously assumed plant growth temperature limit. Black circles show observations of the rate of photosynthesis as a function of temperature for *T. oblongiformia* (Prado et al. 2023), which has the highest optimal growth temperature observed in any vascular plant (Björkman et al. 1972). The green curve is a cubic spline fit to the *T. oblongiformia* data, providing an estimate of 336 K for the extremophile’s upper temperature limit. The dashed blue line shows the 323 K upper temperature limit for land plants that previous studies have used, which is contradicted by the observed ability of *T. oblongiformia* to photosynthesize at a high rate at that temperature. The solid blue line is at 338 K, the maximum temperature at which the panic grass *Dichantheium lanuginosum* has been shown to be able to survive repeated longterm exposure when inoculated with a symbiotic virus-infected root fungus (Redman et al. 2002; Márquez et al. 2007). That is the temperature limit for land plants that we assume in this study.

inactive below 323 K (Salvucci et al. 2001), which is thought to be one of the primary drivers of photosynthetic inhibition under temperature stress (Salvucci & Crafts-Brandner 2004; Scafaro et al. 2023). Nonetheless, there is significant variation in thermotolerance of these enzymes among clades (Salvucci & Crafts-Brandner 2004; Shivhare & Mueller-Cajal 2017; Perkins 2021), with more thermotolerant forms directly resulting in higher optimal growth temperatures for plants (Salvucci & Crafts-Brandner 2004; Scafaro et al. 2019). Furthermore, cyanobacteria in hot springs utilizing the same basic photosynthetic machinery have been found to operate at temperatures as high as 347 K (74 C) (Miller et al. 2013), demonstrating there is no fundamental ceiling for photosynthesis as a mechanism below that temperature. Given the apparent ability of plants in certain conditions to survive repeated exposures of 338 K, in this paper we take this as the upper temperature limit for plants, while including some calculations and remarks on the implications for our results if the tradition plant growth limit of 323 K is retained.

2.2. Weathering model

We adopt a standard expression (Walker et al. 1981; Abbot 2016) for silicate weathering as a function of surface temperature (T) and soil $p\text{CO}_2$ (p_{soil}):

$$\frac{W}{W_{\text{ref}}} = \frac{V}{V_{\text{ref}}} = \exp\left(\frac{T - T_{\text{ref}}}{T_e}\right) \left(\frac{p_{\text{soil}}}{p_{\text{soil,ref}}}\right)^\beta \quad (1)$$

where W [mol yr^{-1}] is the global silicate weathering rate; T_e [K] is the e-folding temperature for weathering; β is the exponent for the power-law dependence on soil CO_2 ; T [K] and p_{soil} [bar] are defined as above; $V_{\text{ref}} = W_{\text{ref}} = 7.5 \times 10^{12}$ moles of CO_2 per year is modern Earth’s approximate CO_2 outgassing rate (Haqq-Misra et al. 2016); $T_{\text{ref}} = 288$ K is the pre-industrial Earth’s global-mean temperature; $p_{\text{soil,ref}} = 2.8 \times 10^{-3}$ bars (since the modern biota maintains soil CO_2 at approximately an order of magnitude higher level than atmospheric CO_2 (Volk 1987)). We test the full range of T_e and β values described in Section 1, using $T_e \in [12.1, 48]$ K and $\beta \in [0.05, 0.91]$ for our calculations. We note that, if global runoff is linearly dependent on temperature as is often assumed (Abbot et al. 2012; Abbot 2016; Graham & Pierrehumbert 2020; Coy 2022), then Taylor expanding the above equation with respect to T and keeping the linear term produces a model equivalent to a global-mean version of the hydrologically-regulated weathering model

of Maher & Chamberlain (2014) (MAC) in the runoff-limited regime (Graham & Pierrehumbert 2020), such that simulations with small T_e are equivalent to the MAC model. If the coupling of climate to weathering emerges from the relationship between runoff and global surface temperature rather than silicate dissolution kinetics (Godsey et al. 2009; Maher & Chamberlain 2014; Graham & Pierrehumbert 2020), then we estimate $T_e \approx 15\text{--}44$ K from modeled temperature sensitivities of high and low latitude rivers (Manabe et al. 2004; Maher & Chamberlain 2014). So, our results should still apply even if the MAC model is a more mechanistically accurate model of weathering than the exponential formulation we are using here.

Taking a logarithm of equation 1 shows that for simulations with the reference outgassing rate ($V = V_{\text{ref}}$), the trajectory is determined by the product of β and T_e , i.e. simulations with $T_e = 20$ K and $\beta = 0.25$ produce the same trajectories as simulations with $T_e = 10$ K and $\beta = 0.5$:

$$\log\left(\frac{V}{V_{\text{ref}}}\right) = \frac{T - T_{\text{ref}}}{T_e} + \beta \log\left(\frac{p_{\text{soil}}(T, p_{\text{atm}})}{p_{\text{soil,ref}}}\right)$$

$$\frac{T_{\text{ref}} - T}{\log\left(\frac{p_{\text{soil}}(T, p_{\text{atm}})}{p_{\text{soil,ref}}}\right)} = T_e \beta$$

so we label results for widely varying T_e and β by the product of the two weathering parameters ($\beta \times T_e$) in some of the results below.

2.3. Soil CO_2 model

Soil $p\text{CO}_2$ (p_{soil}) is maintained above its atmospheric level by below-ground respiration of plant and fungal organic matter; we parameterize this effect as a function of atmospheric $p\text{CO}_2$ (p_{atm}) and NPP following Volk (1987):

$$\frac{p_{\text{soil}}}{p_{\text{soil,ref}}} = R_{\text{NPP}} \left(1 - \frac{p_{\text{atm,ref}}}{p_{\text{soil,ref}}}\right) + \frac{p_{\text{atm}}}{p_{\text{soil,ref}}} \quad (2)$$

where p_{atm} [bars] is the atmospheric $p\text{CO}_2$; $p_{\text{atm,ref}} = 2.8 \times 10^{-4}$ bars CO_2 is the pre-industrial atmospheric CO_2 partial pressure; R_{NPP} is the total net primary productivity relative to modern; and other variables are defined as above. We note that if rates of organic decay are strongly temperature-dependent, then p_{soil} might be sustained at values significantly higher or lower than those given in our study.

2.4. C_3 and C_4 plant productivity models

Relative net primary productivity (R_{NPP}) is taken to be a linear sum of the NPP values predicted by idealized C_3 and C_4 photosynthesis models, relative to model output for modern pre-industrial T and p_{atm} and normalized to estimates of the modern fractions of organic carbon fixation by each pathway:

$$R_{\text{NPP}}(T, p_{\text{atm}}) = f_{\text{C}_3, \text{modern}} R_{\text{NPP}, \text{C}_3}(T, p_{\text{atm}}) + f_{\text{C}_4, \text{modern}} R_{\text{NPP}, \text{C}_4}(T, p_{\text{atm}})$$

$$= 0.725 \frac{NPP_{\text{C}_3}(T, p_{\text{atm}})}{NPP_{\text{C}_3}(288\text{K}, 280 \times 10^{-6} \text{bar})} + 0.275 \frac{NPP_{\text{C}_4}(T, p_{\text{atm}})}{NPP_{\text{C}_4}(288\text{K}, 280 \times 10^{-6} \text{bar})}$$

where $f_{\text{C}_3, \text{modern}} = 0.725$ and $f_{\text{C}_4, \text{modern}} = 0.275$ are the modern fractions of organic carbon fixation by C_3 and C_4 plants respectively according to models of glacial-interglacial changes in global primary productivity during the current ice age (François et al. 1998; Blunier et al. 2012) and $NPP_{\text{C}_3}(T, p_{\text{atm}})$ and $NPP_{\text{C}_4}(T, p_{\text{atm}})$ are C_3 and C_4 productivities in $\mu\text{mol s}^{-1}$ per unit leaf area from biochemical models of photosynthetic CO_2 assimilation for each plant type.

For C_3 plants, we apply a version of the biochemical leaf photosynthesis model from Farquhar et al. (1980). We use temperature response functions from Bernacchi et al. (2001). For simplicity, we assume C_3 photosynthesis is always limited by Rubisco carboxylation (as opposed to other potentially limiting processes like RuBP regeneration or triose-phosphate utilization (Farquhar et al. 1980)), since photosynthesis is commonly limited by Rubisco's kinetics in nature (Rogers & Humphries 2000; Bernacchi et al. 2001):

$$NPP_{\text{C}_3}(T, p_{\text{atm}}) = \left(1 - \frac{\Gamma_*(T)}{C_i(T, p_{\text{atm}})}\right) \frac{V_{\text{c,max}}(T) C_i(T, p_{\text{atm}})}{(C_i(T, p_{\text{atm}}) + K_c(T) \left(1 + \frac{O}{K_o(T)}\right))} - R_d(T) \quad (3)$$

where $\Gamma_*(T) = \exp(19.02 - 37.83/(RT))$ is the CO_2 compensation point for C_3 plants in the absence of respiration, given as a CO_2 concentration in air [$\mu\text{mol mol}^{-1}$]; $C_i(T, p_{\text{atm}})$ is intercellular CO_2 concentration [$\mu\text{mol mol}$] maintained

by exchange of air and water through leaf stomata; $V_{c,\max}(T) = V_{c,\max}(298\text{K}) \exp(26.35 - 65.33/(RT))$ is the maximum rate of carboxylation by Rubisco [$\mu\text{mol m}^{-1} \text{s}^{-1}$] at a given leaf temperature T (assumed equal to global-mean surface temperature in our models); $V_{c,\max}(298) = 57.05 \mu\text{mol m}^{-1} \text{s}^{-1}$ is maximum carboxylation rate at 298 K for *Pinus taleda* (Lin et al. 2012) (a randomly chosen C_3 plant); $K_c = \exp(38.05 - 79.43/(RT))$ [$\mu\text{mol mol}^{-1}$] and $K_O = \exp(20.30 - 36.38/(RT))$ [mmol mol^{-1}] are Rubisco’s temperature-dependent Michaelis–Menten constants for CO_2 and O_2 respectively; $O = 0.21 \times 10^3$ is the atmospheric concentration of oxygen [mmol mol^{-1}]; and $R_d = \exp(18.72 - 46.39/(R*T))$ is mitochondrial respiration in illuminated conditions [$\mu\text{mol m}^{-2} \text{s}^{-1}$]. C_i is calculated with a simple stomatal conductance model drawn from the corrected version of Medlyn et al. (2011, 2012). We assume a constant humidity deficit between air and intercellular spaces of leaves and a constant marginal water cost of carbon (λ) and we apply parameter values for the Duke pine (a C_3 plant) from Lin et al. (Lin et al. 2012):

$$C_i = C_a \frac{g_1}{g_1 + \sqrt{D}} \quad (4)$$

where C_a is the CO_2 concentration in air [$\mu\text{mol mol}^{-1}$]; $D = 2.5 \text{ kPa}$ is an arbitrary assumed constant humidity deficit between the saturated intercellular space of the leaves and the surrounding air (results are not sensitive to its precise value); and

$$g_1 = 10.96 \sqrt{\frac{\Gamma_*(T)}{\Gamma_*(28.1)}}$$

is a fitting parameter that is proportional to $\sqrt{\Gamma_*(T)\lambda}$ (see equation (11) in Medlyn et al. (2011)), scaled with a constant λ to the value of $g_1 = 10.96$ at 28.1 K given for the Duke pine in Lin et al. (2012).

We use a different productivity model for C_4 plants which accounts for the fact that C_4 photosynthesis is nearly insensitive to CO_2 at modern-Earth-like levels due to efficient spatial concentration of CO_2 around Rubisco in bundle sheaths, but becomes linearly dependent on CO_2 at low concentrations when the C_4 plant’s bundle sheaths are subsaturated with CO_2 . The transition between these regimes usually occurs around 100 ppmv CO_2 (Collatz et al. 1992; Chen et al. 1994). We handle this by calculating both CO_2 -saturated and CO_2 -subsaturated rates and assuming that the slower of the two at any given T and p_{atm} operates as the limiting factor on photosynthesis (we always assume fully light-saturated photosynthesis because we cannot account for spatial variations in light and because light limitation should become less and less of an issue for plants under a gradually brightening sun):

$$NPP_{C_4}(T, p_{\text{atm}}) = -R_d(T) + \min \begin{cases} A_{\text{CO}_2} & = 1.8 \times 10^4 V(T) \frac{p_i(p_{\text{atm}})}{p_{\text{tot}}} \\ A_{\text{Rubisco}} & = V(T) \end{cases} \quad (5)$$

where $V(T) = V_{\max} 2^{H(T)}$ is the temperature-dependent rate of light- and CO_2 -saturated Rubisco carboxylation [$\mu\text{mol m}^{-2} \text{s}^{-1}$]; $V_{\max} = 39 \mu\text{mol m}^{-2} \text{s}^{-1}$; $H(T) = \frac{(T-298.15)/10}{(1+\exp(0.3(286.15-T)))(1+\exp(0.3(T-309.15)))}$; $p_i = 0.4p_{\text{atm}}$ [bars] is the intercellular CO_2 partial pressure, taken to be 40% of the ambient atmospheric CO_2 as a first approximation based on measurements suggesting an approximately constant offset between ambient and intercellular CO_2 (Wong et al. 1979; Jacobs 1994); $p_{\text{tot}} = 1 \text{ bar}$ is the total atmospheric pressure; and as suggested in Collatz et al. (1992), Rubisco-limited photosynthesis (A_{Rubisco}), CO_2 -subsaturated photosynthesis (A_{CO_2}), and plant respiration ($R_d = 0.021V(T)$) are all assumed to be linearly related (Cox et al. 1998). This simple formulation allows us to explicitly calculate the CO_2 where C_4 plants transition to CO_2 subsaturation in our model, $p_{\text{atm}} = 1/(1.8 \times 10^4)/0.4 = 1.4 \times 10^{-4}$ bars, or 140 ppmv CO_2 , as well as the CO_2 compensation point for C_4 plants, $p_{\text{atm}} = 0.021/(1.8 \times 10^4)/0.4 = 2.9 \times 10^{-6}$ bars, 2.9 ppmv CO_2 . The transition between CO_2 saturation and subsaturation for C_4 plants is visible in Fig. 3 as a discontinuity in the slope of all carbon cycle trajectories at 140 ppmv CO_2 .

To examine whether the productivity model produces reasonable responses to changes in climate, we compared our results against relative productivity values inferred from ice cores for glacial-interglacial changes in CO_2 and temperature over the past 800,000 years (Yang et al. 2022). Ocean productivity is estimated to have been within 20% of its modern value over the last 400,000 years (Blunier et al. 2012), suggesting the large productivity changes inferred by Yang et al. (2022) are largely attributable to the land biosphere, facilitating comparison with our model. Yang et al. (2022) found glacial productivity minima between 55 and 87% of modern for conditions $\approx 5 \text{ K}$ cooler than today with $\text{CO}_2 \approx 200 \text{ ppmv}$. Our model produces an equivalent result: with $T = 283 \text{ K}$ and $p_{\text{atm}} = 2 \times 10^{-4} \text{ bar}$, $R_{\text{NPP}} = 0.56$, which falls within the inferred range and suggests our model at least qualitatively captures the global response of plant productivity to changes in climate.

2.5. Climate model

The climate model assumes global-mean radiation balance between the planet’s absorbed solar radiation and outgoing longwave radiation:

$$ASR = OLR \quad (6)$$

where ASR is absorbed solar radiation and OLR is outgoing longwave radiation. ASR is defined by:

$$ASR = (1 - a) \frac{S}{4} \quad (7)$$

where $a = 0.29$ is the planetary Bond albedo (Stephens et al. 2015), assumed constant in our model due to uncertainty in the magnitude and direction of the cloud feedbacks that dominate planetary albedo response to changes in CO_2 and insolation (Leconte et al. 2013; Wolf & Toon 2014, 2015; Popp et al. 2016; Wolf et al. 2018), and S is the top-of-atmosphere substellar insolation, divided by a factor of 4 to account for the distribution of radiation intercepted by Earth’s circular silhouette across its spherical surface. S is related to time in the future by interpolation of luminosity vs. time data from a standard stellar evolution calculation presented in Bahcall et al. (2001). OLR is defined using the fit to H_2O -saturated radiative-convective column models presented in Caldeira & Kasting (1992) with an additional tuning factor of -18 W m^{-2} to reproduce Earth’s climate with the modern albedo $a = 0.29$ at the modern insolation of $S = 1361 \text{ W m}^{-2}$:

$$OLR = \sigma T_{\text{eff}}^4 - 18 \quad (8)$$

where σ is $5.67 \times 10^{-8} \text{ W m}^{-2} \text{ K}^{-4}$ and T_{eff} is Earth’s effective radiating temperature. T_{eff} is defined by:

$$T_{\text{eff}} = T - \Delta T \quad (9)$$

where T is the global-mean surface temperature and ΔT is the warming due to the greenhouse effect, a polynomial fit to output from radiative-convective column model simulations provided by Caldeira & Kasting (1992):

$$\Delta T = 815.17 + \frac{4.895 \times 10^7}{T^2} - \frac{3.9787 \times 10^5}{T} - \frac{6.7084}{(\log(p_{\text{atm}}))^2} + \frac{73.221}{\log(p_{\text{atm}})} - \frac{3.0882 \times 10^4}{T \log(p_{\text{atm}})} \quad (10)$$

where T is Earth’s global-mean surface temperature in Kelvin and p_{atm} is the atmospheric CO_2 partial pressure in bars.

3. RESULTS

First, we compare future biosphere trajectories with parameterizations that represent the two classes of land plant extinction— CO_2 starvation and overheating. The parameterization leading to extinction from inadequate carbon dioxide follows Caldeira & Kasting (1992) (henceforth CK92), who used $T_e = 13.7 \text{ K}$ and $\beta = 0.25$. The parameterization leading to overheating relies on the study of Krissansen-Totton & Catling (2017) (henceforth KT17), who constrained the distributions of T_e and β values that are consistent with paleoclimate proxy records. We use their median $T_e = 31 \text{ K}$ and $\beta = 0.41$ values, which were drawn from a Michaelis-Menten weathering formulation often used to approximate the impact of vascular plants on weathering rates (Volk 1987). Together, these two simulations display the main qualitative properties of the two classes of land plant extinction trajectories.

The KT17 parameters result in a longer future lifespan of terrestrial plants relative to the CK92 parameters (1.8 and 1.3 Gyr, respectively, Fig. 2A). The stronger dependence of the silicate weathering rate on temperature (smaller T_e) with CK92 parameters leads to a stronger response to increased luminosity, monotonically decreasing atmospheric CO_2 concentration and ultimately leading to plant extinction by CO_2 starvation. In contrast, the weaker temperature dependence (larger T_e) with the KT17 parameters results in higher atmospheric CO_2 levels for a given solar luminosity (Fig. 2B), avoidance of plant starvation, and ultimate extinction by overheating. The 1.3 Gyr lifespan that we calculate with the CK92 parameterization is substantially longer than the 0.9 Gyr calculated in the original study because in our model C_4 plants have a lower compensation threshold (2.9 ppmv, rather than 10 ppmv). With a threshold of 10 ppmv, as assumed in previous biosphere lifespan studies, the difference between the CK92 and KT17 lifespans is even larger: $\approx 0.9 \text{ Gyr}$ as opposed to $\approx 1.8 \text{ Gyr}$.

In both simulations, C_3 plant productivity monotonically decreases, but in the CK92 simulation C_3 extinction occurs after 0.5 Gyr, while in the KT17 simulation they last for 0.8 Gyr (Fig. 2A), as the CO_2 decrease with

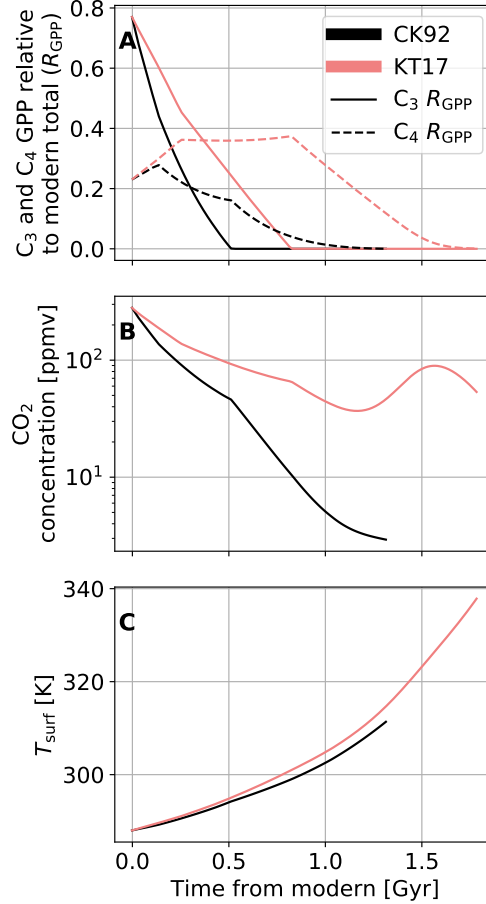


Figure 2. Representative future climate and biosphere trajectories. (A) Trajectories of C₃ (solid) and C₄ (dashed) plant productivity relative to total modern productivity. (B) Atmospheric CO₂ concentration (ppmv). (C) Surface temperature (T_{surf} in Kelvins). Results are shown with weathering parameters from Caldeira & Kasting (1992) (black, $T_e = 13.7$ K, $\beta = 0.25$) and from Krissansen-Totton and Catling (Krissansen-Totton & Catling (2017) (pink, $T_e = 31.0$ K, $\beta = 0.41$).

increasing luminosity is less pronounced. In both cases, the fall in C₃ productivity reduces soil respiration, decreasing soil CO₂ (p_{soil} in Eq. 1 and 2). This reduces the biotic acceleration of weathering and slows the drawdown of CO₂ with increasing solar luminosity, extending the lifespan of C₃ plants by delaying starvation. This is reflected in the shallow slope of the CO₂ vs. time curve for each simulation when C₃ plants exist (Fig. 2B). The delayed CO₂ decrease also sustains C₄ productivity at high levels for long periods in both simulations (Fig. 2A).

Initially, during the period when C₄ plants operate without CO₂-limitation, their productivity is insensitive to changes in atmospheric composition. Over this interval, increasing temperature leads to climbing C₄ productivity. Only after 0.12 (CK92 parameters) or 0.25 Gyr (KT17 parameters) does CO₂ limitation of photosynthesis begin to outweigh temperature fertilization for C₄ plants in our simulations. With the CK92 parameters, C₄ productivity begins to fall after 0.12 Gyr, whereas with the KT17 parameters, C₄ productivity stabilizes at 0.25 Gyr at a value for which the reduction from gradually decreasing CO₂ is approximately balanced by the increase from warming temperatures. C₄ productivity remains at this high value until C₃ plants die off, at which point atmospheric composition begins to change more rapidly because the C₃ productivity decrease can no longer reduce p_{soil} and alter the weathering rate. This causes C₄ productivity to finally start declining 0.8 Gyr from now, falling below its present value only after 1.1 Gyr.

As C₄ productivity falls after 0.8 Gyr in the KT17 simulation, the CO₂ decrease is initially rapid but slows with time, until around 1.1 Ga it halts and then reverses. This is due to the same fundamental mechanism as the initial decelerated loss of CO₂ from decreasing C₃ productivity during the first few hundred million years described above.

As C_4 productivity falls, root respiration slows (p_{soil} approaches p_{atm} in Eq.2), necessitating higher temperature and atmospheric CO_2 levels to maintain a given weathering rate. With the large T_e in KT17, an atmospheric CO_2 increase becomes necessary to offset the decline in weathering rate from declining productivity, and only after temperatures climb past 327 K at 1.6 Gyr does the temperature effect on weathering begin to dominate and resume net CO_2 drawdown. In contrast to the rolling trajectory displayed by the KT17 simulation, CO_2 in the CK92 simulation falls faster and monotonically with time, leading to cooler conditions. The smaller values of T_e and β in the CK92 parameterization require a smaller temperature change and a larger CO_2 change to sustain a given weathering rate upon a change in solar luminosity.

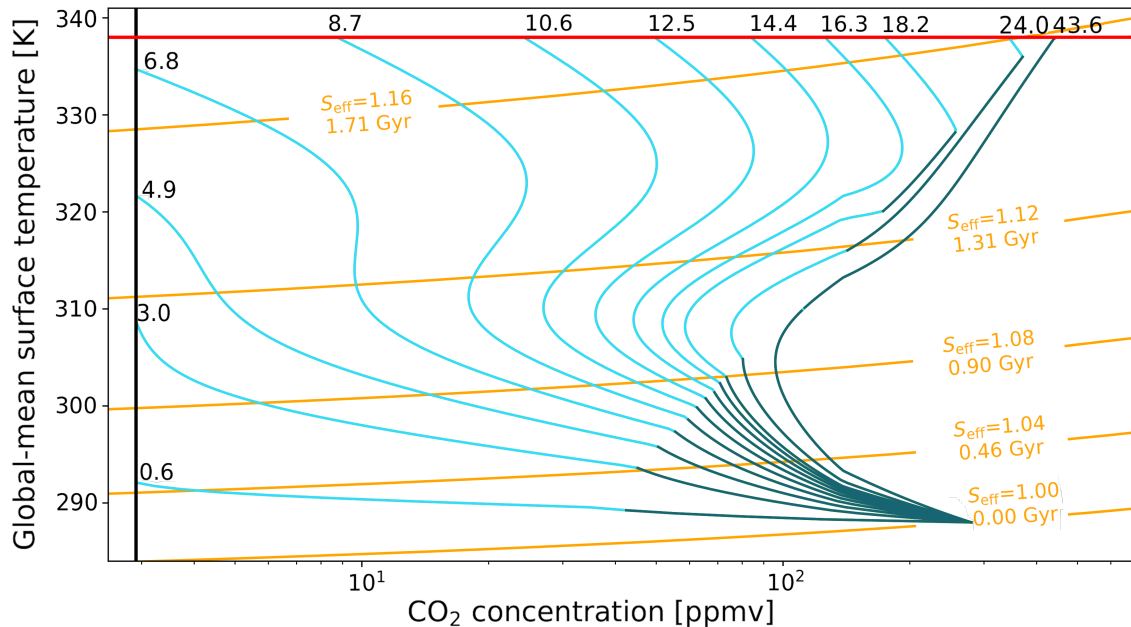


Figure 3. Climate trajectories in CO_2 (ppmv)-temperature (Kelvins) space with modern outgassing for different values of $T_e \times \beta$ (Kelvins). Blue curves (both light and dark) show temperature- CO_2 combinations that produce carbon cycle equilibrium at modern outgassing for different combinations of weathering parameters. Each blue curve is labeled by its corresponding $T_e \times \beta$ value. Dark blue portions of the curves have both C_3 and C_4 plants, while light blue portions have only C_4 plants. The horizontal red line marks our assumed temperature threshold for land plants, 338 K (Redman et al. 2002; Márquez et al. 2007; Clarke 2014). The vertical black line marks the CO_2 compensation point for C_4 plants that emerges from our photosynthesis model, 2.9 ppmv. Orange contours show temperature- CO_2 combinations that produce top-of-atmosphere radiative equilibrium at a given effective insolation (S_{eff}) and corresponding time in the future, so time and insolation increase from the bottom-right to the top-left of the figure.

For modern outgassing, model trajectories are determined by the product of β and T_e (K), rather than each parameter independently (Fig. 3; section 2.2). For $\beta \times T_e \in [0.6, 43.6]$ within estimates of the plausible range (Krissansen-Totton & Catling 2017; Deng et al. 2022), we find substantial variation not only in timing of biosphere demise, but also in kill mechanism. For relatively high temperature sensitivity (low T_e) and/or low CO_2 sensitivity (low β), like CK92, the biosphere dies by CO_2 starvation after monotonic or nearly monotonic drawdown of CO_2 to 2.9 ppmv (the C_4 compensation point; Eq. 5). For settings like KT17, with high T_e and/or high β , the biosphere overheats at 338 K after a non-monotonic atmospheric evolution driven by the shifting balance between the contrasting effects of increasing temperature and decreasing soil CO_2 on the weathering rate, as described above.

For most parameter values, C_3 plants die off permanently from CO_2 starvation, leaving behind biospheres entirely consisting of C_4 plants. The CO_2 at which this occurs varies among the trajectories because the C_3 CO_2 compensation point is temperature-dependent (Eq.3), with lower temperatures allowing C_3 plants to persist to lower CO_2 levels (Farquhar et al. 1980). In the simulations with $T_e \times \beta = 18.2$ K and 24.0 K, CO_2 eventually reaches high enough levels

during the increasing phase that C_3 plants are able to re-emerge far in the future, delaying the onset of the CO_2 decrease at the end of each trajectory. In the simulation with $T_e \times \beta = 43.6$ K, CO_2 only briefly falls to levels low enough for C_3 plants to disappear, so they remain present almost continuously until the biosphere overheats at a CO_2 of 440 ppmv with no final CO_2 decrease. In this limit, the silicate weathering feedback is almost entirely mediated by p_{soil} , which is in turn determined largely by Net Primary Productivity (NPP), so that a balanced carbon cycle requires maintaining near-modern NPP levels throughout the simulation, which is why CO_2 remains high.

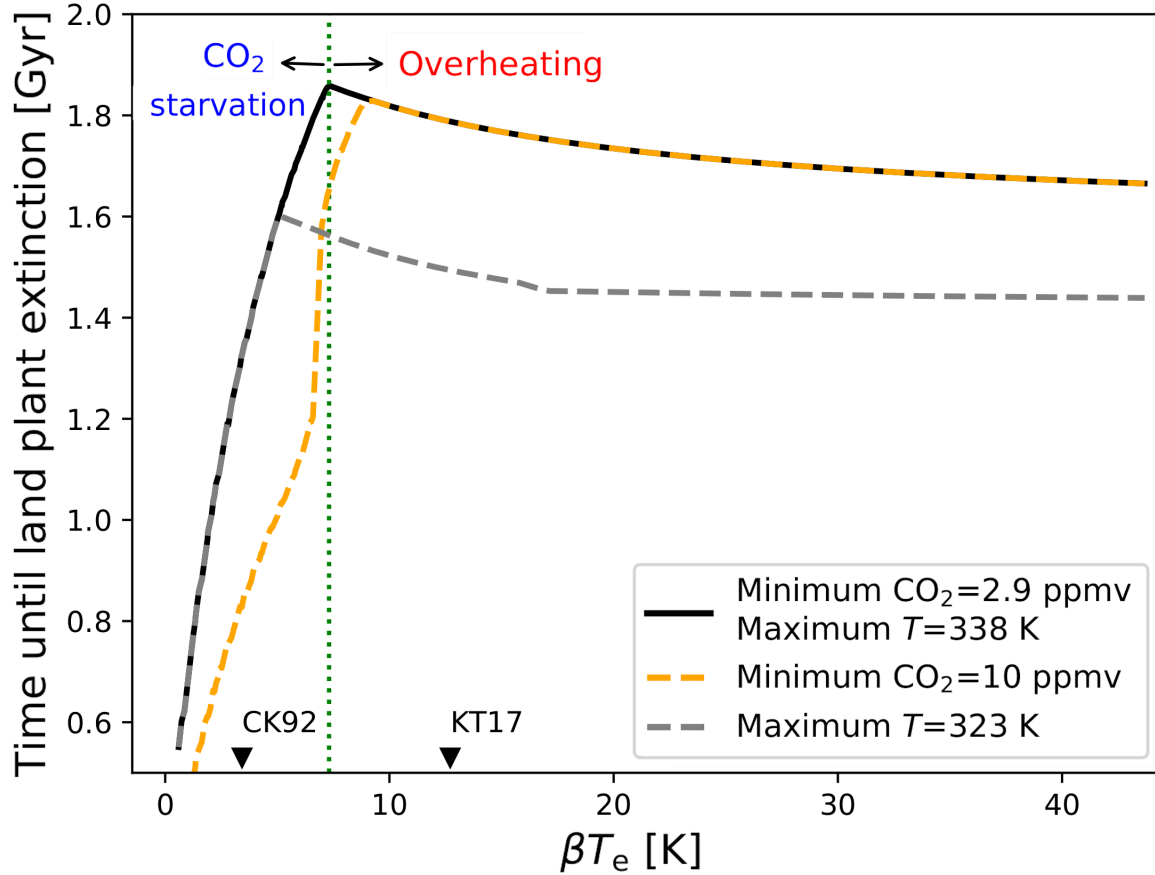


Figure 4. Future lifespan of the complex biosphere [Gyr] as a function of $T_e \times \beta$ [K] with modern CO_2 outgassing. The black curve records lifespans with our 338 K temperature threshold and the 2.9 ppmv CO_2 threshold that emerges from our C_4 photosynthesis model. The vertical green dotted line separates the trajectories that end in CO_2 starvation for land plants from the trajectories that end in overheating. The grey dashed line shows the time required for our model to reach either our standard CO_2 threshold or 323 K, the temperature threshold used by prior studies. The orange dashed line shows the time required for our model to reach either our standard temperature threshold or 10 ppmv CO_2 , the CO_2 minimum assumed by most prior studies.

In the CO_2 starvation regime, small variations in T_e and β lead to large changes in expected lifespan (Fig. 4), with increases in β or T_e both increasing lifespan by raising the equilibrium CO_2 at a given insolation, delaying starvation. With our climate model, lifespans in the CO_2 starvation regime range from 0.55 Gyr at $T_e \times \beta = 0.6$ to a maximum lifespan of 1.86 Gyr at $T_e \times \beta = 7.3$, which marks the transition from CO_2 starvation to overheating. At $T_e \times \beta > 7.3$, the plant lifespan shortens with increasing $T_e \times \beta$ because elevated CO_2 causes the planet to reach the 338 K threshold earlier, falling from 1.86 Gyr at $T_e \times \beta = 7.3$ to 1.66 Gyr at $T_e \times \beta = 43.6$ K. A CO_2 compensation point of 10 ppmv (orange dashed curve, Fig. 4) or upper temperature threshold of 323 K (grey dashed curve, Fig. 4) can each shorten lifespans by a few hundred million years.

So far, all presented simulations have assumed outgassing and land fraction equal to modern values, but in the far future geodynamic effects may reduce Earth’s CO₂ outgassing rate and drive continental growth (Franck et al. 2000). Both changes would reduce the equilibrium CO₂ of the atmosphere, hastening CO₂ starvation (Franck et al. 1999, 2000; Lenton & von Bloh 2001). To test this possibility, we calculate the lifespan of land plants under different constant outgassing rates. In our zero-dimensional carbon cycle model, a given reduction in outgassing is equivalent to an increase in continental area or weatherability by the same factor at constant outgassing.

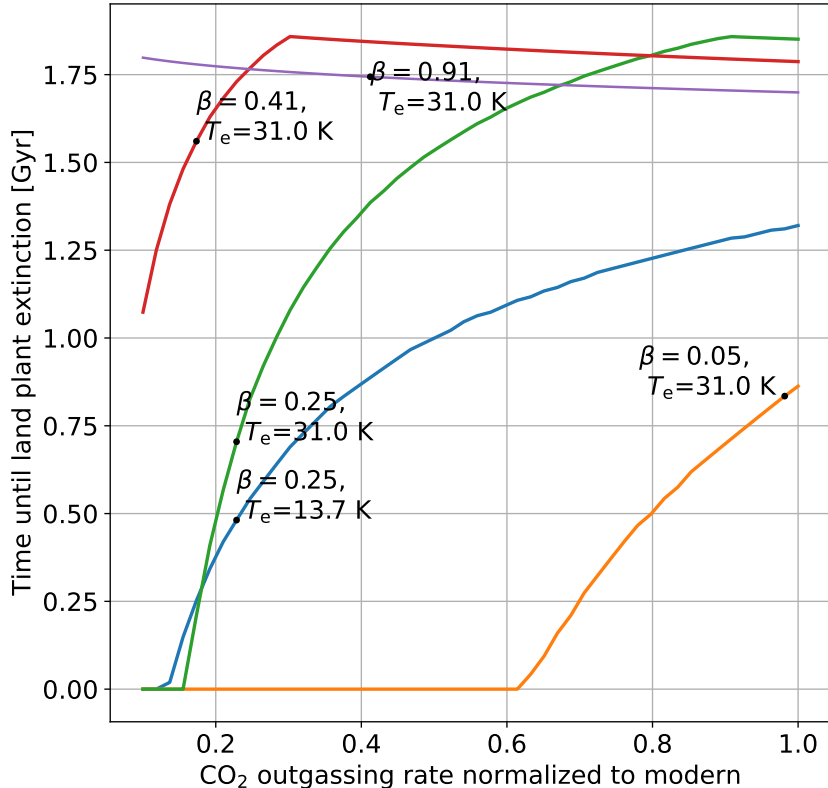


Figure 5. Time until land plant extinction [Gyr] vs. CO₂ outgassing rate relative to modern for varying weathering parameters. The purple curve has $T_e=31.0$ K and $\beta=0.91$, red has $T_e=31.0$ K and $\beta=0.41$, orange has $T_e=31.0$ K and $\beta=0.05$, green has $T_e=31.0$ K and $\beta=0.25$, and blue has $T_e=13.7$ K and $\beta=0.25$.

The effect of outgassing on biosphere lifespan depends strongly, and independently, on β and T_e (instead of just on their product). To demonstrate the variety in the response, we display biosphere lifespans as a function of outgassing rates down to 10% of modern for a few combinations of weathering parameters (Fig. 5). For simulations that die by overheating at modern outgassing (red curves in Fig. 5), decreasing the outgassing rate initially causes an increasing lifespan by delaying the time of overheating. The delay lasts until the outgassing rate at which overheating coincides with the CO₂ starvation threshold is approached for a given set of parameters, producing a maximum lifespan of 1.86 Gyr. For very strong CO₂-dependence and weak temperature-dependence (e.g., with $\beta = 0.91$, $T_e = 31.0$ K), even a reduction in outgassing of 90% relative to modern does not shorten the lifespan at all. Changes in outgassing rate are, therefore, not likely to alter our conclusion that thermal stress is the more likely kill mechanism for the complex biosphere. In contrast, for outgassing rates and weathering parameters that produce CO₂ starvation (blue curves in Fig. 5), any reduction in outgassing dramatically decreases the lifespan by allowing the minimum CO₂ for C₄ plants to be reached earlier.

4. DISCUSSION

4.1. *Potential implications for life beyond Earth*

The future lifespan of the complex biosphere plays a key role in a body of literature that applies observational self-sampling assumptions to explain why technological intelligence appeared late in Earth’s window of habitability and to estimate the number of critical, highly improbable steps in the evolution of intelligent life on Earth (Carter 1983; Hanson 1998a,b; Flombaum 2003; Watson 2004; Carter 2008; Watson 2008; Ćirković et al. 2009; Aldous 2012; Bostrom 2013; Lingam & Loeb 2019; Snyder-Beattie et al. 2021; Hanson et al. 2021; Snyder-Beattie & Bonsall 2022). This statistical picture is frequently referred to as the “Carter model” (e.g. Waltham 2017; Snyder-Beattie et al. 2021) after its originator Brandon Carter (Carter 1983). If the evolution of intelligent observers requires a series of n critical, unlikely evolutionary transitions, each of which would typically be expected to take longer than the habitable lifetime of a planet, then if we condition on the success of all n steps (with the n th step being the evolution of intelligence), the resulting probability density function for the emergence of intelligence as a function of time since the onset of habitability (t) can be written (e.g. Watson 2008):

$$p_{\text{intel}}(t) \approx \frac{nt^{n-1}}{\tau_{\text{hab}}^n} \quad (11)$$

where τ_{hab} is the total duration of planetary habitability and other variables retain their previous definitions. From this, the expectation time for the evolution of an intelligent species can be derived:

$$\begin{aligned} \tau_{\text{intel}} &= \int_0^{\tau_{\text{hab}}} tp_{\text{intel}}(t)dt \\ &= \frac{n}{n+1}\tau_{\text{hab}} \end{aligned} \quad (12)$$

which implies that a larger number n of “hard steps” pushes the evolution of intelligence to later dates in the window of planetary habitability. If we take the emergence of intelligence on Earth to coincide with the emergence of *Homo sapiens*, then the time since the emergence of intelligence (10^5 - 10^6 years; Galway-Witham & Stringer 2018) is small relative to the gigayear timescales of Earth’s biosphere’s history and future, so τ_{hab} is simply the sum of τ_{intel} and the future lifespan of the complex biosphere, which we will denote τ_{future} . With this simplification, we can calculate n as a function of timescales:

$$\tau_{\text{intel}} = \tau_{\text{hab}} - \tau_{\text{future}} \quad (14)$$

$$= \frac{n+1}{n}\tau_{\text{intel}} - \tau_{\text{future}} \quad (15)$$

$$n = \frac{\tau_{\text{intel}}}{\tau_{\text{future}}} \quad (16)$$

meaning a longer future lifespan of the biosphere suggests proportionally fewer hard steps in the evolution of intelligent life (Carter 1983; Hanson 1998a; Carter 2008; Watson 2008; Snyder-Beattie & Bonsall 2022).

Water was flowing on Earth’s surface by 4.4 Ga (Valley et al. 2002; Waltham 2017), so we will take that as the time habitability began on Earth, with $\tau_{\text{intel}} = 4.4$ Gyr following Waltham (2017), though the Late Heavy Bombardment may have prevented lasting habitability until 3.9 Ga (Pearce et al. 2018). With the estimate of $\tau_{\text{future}} \approx 1$ Gyr from Caldeira & Kasting (1992), previous researchers have estimated $n \approx \frac{4.4}{1} \approx 4 - 5$ (Carter 2008; Watson 2008; Waltham 2017). Alternatively, with our longest estimate for the future lifespan of $\tau_{\text{future}} = 1.86$ Gyr, the expected value for n becomes $\frac{4.4}{1.86} \approx 2.4$, suggesting two to three critical steps may be a better estimate. This would suggest that the emergence of intelligent life may be a less difficult (and consequently more common) process than some previous authors have argued (e.g. Snyder-Beattie et al. 2021; Hanson et al. 2021), though since the hard steps can have arbitrarily small probabilities of occurring, intelligent life could still be extremely rare even with just a single hard step.

The Carter model also allows for constraints to be placed on the timing of the hard steps that occurred prior to the advent of intelligence. The probability density function and expected timing for step m of an n -hard-step process can

be written (Watson 2008):

$$p_{m/n}(t) = \frac{n!}{(n-m)!(m-1)!} \frac{t^{m-1}(\tau_{\text{hab}} - t)^{n-m}}{\tau_{\text{hab}}^n} \quad (17)$$

$$\langle t_{m/n} \rangle = \int_0^{\tau_{\text{hab}}} t p_{m/n}(t) dt \quad (18)$$

$$\langle t_{m/n} \rangle = \frac{m}{n+1} \tau_{\text{hab}} \quad (19)$$

where $p_{m/n}(t)$ is the probability density function for step m and $\langle t_{m/n} \rangle$ is the expected time between the onset of habitability and the occurrence of step m . Equation 19 makes it clear that the steps are distributed evenly across the habitable period, with each step separated on average by a duration of $\tau_{\text{hab}}/(n+1)$, which is also the typical amount of time that separates step n from the end of habitability, i.e. $\tau_{\text{hab}}/(n+1) = \tau_{\text{future}}$ and therefore

$$\langle t_{m/n} \rangle = m\tau_{\text{future}}. \quad (20)$$

This equal spacing constraint means that the first hard step ought to take place approximately τ_{future} years after the onset of habitability, which means the future lifespan of the biosphere imposes a timescale that can be used to evaluate whether the amount of time that passed between the onset of habitability and the origin of life on Earth ($\equiv \tau_{\text{OOL}}$) is consistent with expected hard step timing. If $\tau_{\text{future}} \approx \tau_{\text{OOL}}$, then the origin of life is plausibly a hard step, meaning its typical timescale is longer than the typical habitable period of Earth-like planets, suggesting life on other worlds will be rare. Alternatively, if τ_{future} is significantly larger than τ_{OOL} , then this suggests that the origin of life is not a hard step (i.e. it typically happens on a shorter timescale than the lifetime of planetary habitability), which would imply that life might be fairly common in the universe.

The timing of the onset of habitability and the timing of the origin of life on Earth are both somewhat poorly constrained (Pearce et al. 2018), resulting in estimates for τ_{OOL} that could range from ~ 0 Gyr to 0.8 Gyr, depending on which pieces of evidence are taken to confirm the presence of habitability and the presence of life. For example, if we take the the initiation of habitability on Earth to be 4.316 Ga based on an estimate for when water might have flowed on Earth after the Moon-forming impact under the assumption that Earth's magma ocean atmosphere cooled the surface inefficiently and took ~ 0.1 Gyr to reach the condensation point of water at the surface (Pearce et al. 2018) and we take the origin of life to be 4.28 Ga based on putative microfossils in early hydrothermal vent precipitates (Dodd et al. 2017), then $\tau_{\text{OOL}} = 4.316 - 4.28 = 0.036$ Gyr. Alternatively, if we assume that the Earth cooled efficiently after the Moon-forming impact, allowing water to flow earlier, then the start of habitability may have been as far back as 4.5 Ga, and if we take evidence for stromatolites 3.7 Ga as the earliest evidence for life, then $\tau_{\text{OOL}} = 0.8$ Gyr (Pearce et al. 2018).

To quantify how surprising these timings would be if the origin of life was the first hard step in the evolution of intelligence, we can integrate the probability density function $p_{m/n}$ (Equation 17) to derive the cumulative probability $P_{m/n}$ of step $m = 1$ as a function of time, then calculate the two-tailed significance with $2P_{m/n}$ if $P_{m/n} > 0.5$ or $2(1 - P_{m/n})$ if $P_{m/n} < 0.5$ (Waltham 2017). The smaller the calculated significance at a given time, the more surprising it would be for the origin of life to occur at that time, assuming it is a hard step. In the top panel of Figure 6, we plot the significance as a function of the timing of the origin of life with a model assuming $n = 2$ hard steps with $\tau_{\text{future}} = 1.86$ Gyr (corresponding to our max calculation in this paper) and with a model assuming $n = 5$ hard steps and $\tau_{\text{future}} = 1$ Gyr (corresponding to previous calculations, e.g. Watson 2008; Carter 2008; Waltham 2017). The significance for the $n = 5$ scenario ranges from 0.065 (or 6.5%) for $\tau_{\text{OOL}} = 0.036$ Gyr up to a peak of 1 for $\tau_{\text{OOL}} = 0.7$ Gyr and back down to 0.897 for the maximum permitted τ_{OOL} of 0.8 Gyr (blue line, top panel of Fig. 6). Using a common significance threshold of 0.05 (Waltham 2017), none of these origin of life timings would be confidently ruled out in the $n = 5$ scenario, meaning any of these timings would be consistent with the origin of life being a hard step. For the $n = 2$ scenario that arises from the longer future lifespan calculated in this study, the significance rises from 0.029 (2.9%) at $\tau_{\text{OOL}} = 0.036$ Gyr to 0.48 at $\tau_{\text{OOL}} = 0.8$. The $n = 2$ scenario reaches a significance of 0.05 at $\tau_{\text{OOL}} = 0.079$ Gyr, suggesting that if τ_{OOL} were confirmed to lie between 0.036 and 0.079 Gyr, then the $n = 2$ scenario would (very tentatively) suggest that the origin of life is not a hard step and thus may occur commonly on other (exo)planets. The bottom panel shows the ratio of the significance values of the two scenarios through time, demonstrating that the significance for the $n = 5$, $\tau_{\text{future}} = 1$ Gyr scenario is 2-3 times larger than that of the $n = 2$, $\tau_{\text{future}} = 1.86$ Gyr scenario across the given range of τ_{OOL} . These constraints are weak, but this suffices to show

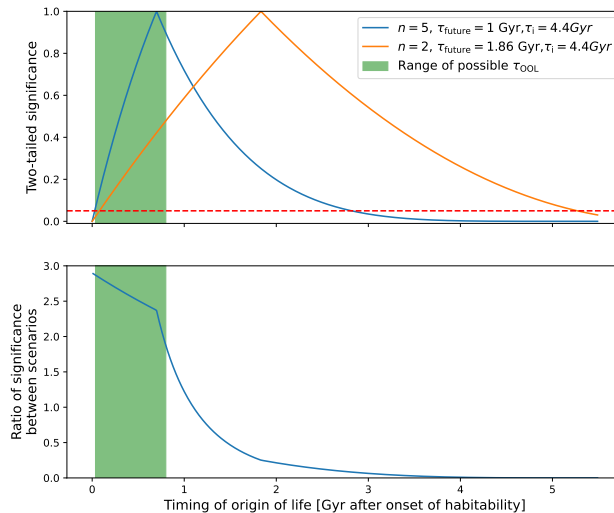


Figure 6. Significance and ratio of significance as a function of origin of life timing for two different values of the future lifespan of the biosphere and number of “hard steps” in the evolution of intelligence, assuming the origin of life was the first hard step. (Top panel) The blue curve shows the significance as a function of timing for the origin of life as the first hard step in a $n = 5$ hard step process in which $\tau_{\text{future}} = 1$ Gyr. The orange curve shows the significance as a function of timing for the origin of life as the first hard step in a $n = 2$ hard step process in which $\tau_{\text{future}} = 1.86$ Gyr. The red dashed line denotes a 0.05 significance threshold. The shaded green area in the top and bottom panels shows a range of τ_{OOL} permitted by evidence for the onset of habitability for Earth (defined by e.g. the first flowing water) and early evidence for the presence of life. The bottom panel shows the ratio of the significance values for the two scenarios described above, demonstrating that the likely τ_{OOL} values are somewhat more surprising in the $n = 5$ case, though not overwhelmingly so.

that a longer τ_{future} may provide weak evidence that the origin of life is a common process, essentially by suggesting that intelligence arose less late in Earth’s history than previously thought. Future investigations in the Carter model framework should account for the lengthened τ_{future} suggested by this study.

It may also be astrobiologically significant that a temperature upper bound for vascular plants of 338 K (Redman et al. 2002; Márquez et al. 2007) may allow some forms of complex land life to survive to Earth’s moist or runaway greenhouse transition (Kasting et al. 1993; Leconte et al. 2013; Wolf & Toon 2014, 2015). 3D climate models differ in their prediction of climate evolution at high insolation and low CO_2 (Leconte et al. 2013; Wolf & Toon 2014, 2015; Popp et al. 2016; Wolf et al. 2018; Goldblatt et al. 2021; Yan et al. 2022), with a range that includes our 0D climate model. The moist greenhouse climate state (in which Earth’s tropopause cold trap becomes less efficient, allowing the stratosphere to become moist and triggering geologically rapid loss of water to space) has been predicted to occur at surface temperatures ranging from 332 K (Wolf & Toon 2015) to 350 K (Kasting et al. 2015), meaning our threshold temperature for plant death approximately coincides with a possible mechanism for the loss of Earth’s habitability. Similarly, the runaway greenhouse (in which Earth’s ocean evaporates into the atmosphere at insulations above a critical threshold due to a limit on outgoing longwave radiation imposed by the interplay between water vapor’s greenhouse effect and its exponential temperature sensitivity) has been estimated to occur at insulations between $S_{\text{eff}} \approx 1.1$ (Leconte et al. 2013) (corresponding to 1.1 Gyr in the future) and $S_{\text{eff}} > 1.21$ (Wolf & Toon 2015) (corresponding to > 2.19 Gyr in the future). Our predicting timings for land plant extinction also fall within this range of potential future runaway greenhouse timings. Therefore, an important implication of our work is that the factors controlling Earth’s transitions into exotic hot climate states could be a primary control on the lifespan of the complex biosphere, motivating further study of the moist and runaway greenhouse transitions with 3D models. Generalizing to exoplanets, this suggests that the inner edge of the “complex life habitable zone” may be coterminous with the inner edge of the classical circumstellar habitable zone, with relevance for where exoplanet astronomers might expect to find plant biosignatures like the “vegetation red edge” (Seager et al. 2005).

4.2. Caveats

Our use of global-mean models prevents the representation of inherently 2- and 3-dimensional phenomena important for climate, silicate weathering, and plant growth. For example, 3D global climate model simulations suggest that spatially complex cloud feedbacks play a crucial role in determining the surface temperatures of hot, high-insolation climates like those expected in Earth’s far future (Wolf & Toon 2015; Goldblatt et al. 2021; Yan et al. 2022). The global-mean framework also obscures the fact that higher latitudes and altitudes tend to be cooler than the planet’s mean temperature, potentially allowing land plants (and the organisms they sustain) to persist in shrinking polar and mountain refugia long past the point where Earth’s global-mean temperature exceeds the temperature threshold for land plants (“Swansong biospheres;” O’Malley-James et al. 2013). Alterations in albedo and hydrological cycling driven by changes in the relative fractions of land covered by vegetation and desert as plant productivity falls may also influence Earth’s far-future temperature and CO₂ trajectories (Kleidon et al. 2000). Additionally, the total global silicate weathering rate (and therefore the climate equilibrium of the carbon cycle) is sensitive to the spatial distribution of land on the planet (Baum et al. 2022). A more computationally intensive modeling framework—e.g. a global climate model coupled to an interactive land model with dynamic vegetation—would be necessary to resolve effects like these and quantify their impact on the future lifespan of the biosphere.

Furthermore, even by the standards of global-mean parameterizations, the climate model we utilize in this study is quite simple and excludes several potentially relevant physical processes. For example, we assume a constant planetary Bond albedo of $a = 0.29$, ignoring the potential for the loss of sea ice and accumulation of atmospheric water vapor to darken the planet under higher surface temperatures, positive feedbacks that which would accelerate warming and reduce the time required to reach either CO₂ starvation or the overheating threshold. We consider this justified for an idealized, global-mean climate model in the high-insolation regime studied here because, as noted in Section 4.1, state-of-the-art 3D GCMs disagree in their predictions about Earth’s climate response to increased insolation, particularly with respect to the impact of clouds on planetary albedo and longwave emission, which may have a destabilizing effect or a stabilizing effect on surface temperatures in response to the combination of increased insolation and decreased CO₂ (Leconte et al. 2013; Wolf & Toon 2014, 2015; Popp et al. 2016; Wolf et al. 2018; Goldblatt et al. 2021; Yan et al. 2022).

Given the spread in predicted climates in state-of-the-art simulations, our model provides adequate estimates despite its various grave simplifications. For example, Leconte et al. (2013) used the the LMD GCM to predict a global-mean surface temperature of ≈ 335 K with an Earth-like 1 bar N₂ atmosphere and CO₂ of 375 ppmv at $S_{\text{eff}} = 1.1$, with any further increases to S_{eff} triggering a runaway greenhouse in their GCM, while Wolf et al. (2018) predicted a global-mean surface temperature of only 307 K for nearly the same conditions with 360 ppmv CO₂ using the Community Atmosphere Model version 4 (CAM4) GCM. For comparison, our global-mean model predicts a temperature of 311 K at modern insolation and 360 ppmv CO₂, intermediate between the LMD and CAM4 results, though closer to CAM4. Simulations using the Community Atmosphere Model version 3 (CAM3) GCM (Wolf & Toon 2014) produced global-mean surface temperatures of only 312.9 K with $S_{\text{eff}} = 1.15$, 500 ppmv CO₂, and 10 ppmv of CH₄, while our climate model predicts a significantly hotter 333 K temperature under those conditions, even without the extra greenhouse forcing provided by CH₄. Another set of simulations with CAM4 produced significantly warmer results than CAM3 (Wolf & Toon 2015), with CAM4 predicting a temperature of 331.9 K at $S_{\text{eff}} = 1.125$ and 367 ppmv CO₂, while CAM3 predicted ≈ 305 K and our model predicts a temperature of 320.5 K for those conditions. Overall, our model’s predictions fall within the wide range of those produced by more sophisticated GCMs.

Most recent data (combining different subsets of paleoclimate proxy measurements, modern field observations, theoretical calculations, simulations, and laboratory experiments) suggest that silicate weathering is weakly temperature-dependent, with $T_e \sim 30\text{-}40$ K (Maher & Chamberlain 2014; Krissansen-Totton & Catling 2017; Graham & Pierre-humbert 2020; Herbert et al. 2022; Brantley et al. 2023), though one recent study examining the degree of chemical alteration of clays as a function of environmental variables suggested a strong dependence, with $T_e \sim 12.1$ K (Deng et al. 2022). Our work, therefore, cannot rule out with certainty CO₂ starvation as the complex biosphere kill mechanism. Our contribution should be read as a strong indication that the alternative mechanism of overheating is preferred, subject to further investigation of the global functioning of silicate weathering.

We also note that we did not model photosynthesis by the third major photosynthetic pathway prevailing among land plants on Earth, crassulacean acid metabolism (CAM), which is used by roughly 6% of land plant species (Keeley & Rundel 2003). Like C₄ plants, CAM plants concentrate CO₂ in their cells to enhance their rates of photosynthesis, but they use a different method. At night, they open their stomata to intake CO₂, storing the carbon as malic acid.

During the day, stomata are closed to minimize water loss, and carbon is provided to Rubisco for light-driven fixation by decarboxylating the stored malic acid back into CO_2 (e.g. Keeley & Rundel 2003). The strategy is adopted by many desert succulents to combat aridity (Edwards & Ogburn 2012), and it would likely provide an increasingly significant advantage in the increasingly hot, low CO_2 climates expected in Earth’s far future under a brightening Sun, since increased temperature will magnify the rate of evaporation from the plant, and reduced CO_2 will cause plants to open their stomata wider, also increasing water loss. We excluded CAM plants from our analysis for two reasons: first, there is an apparent lack of simple temperature- and CO_2 -dependent biochemical CAM productivity models analogous to those we used for C_3 and C_4 plants; and second, the particular adaptation of CAM plants to arid conditions would have necessitated an explicit model of water cycling, which is even less amenable to global-mean modeling than the existing components of our modeling framework. A 3D GCM coupled to a landscape model with dynamic vegetation would provide a more appropriate framework to test the impact of CAM photosynthesis on the future of land plants and serve as a natural extension of this work.

Finally, environmental tolerance thresholds of land plants may only represent an evolutionary optimum under current conditions, rather than hard physical limits. C_4 photosynthesis, which plays a major role in the ability of the biosphere to survive at low CO_2 in the far future in our calculations, appeared geologically recently, likely sometime in the Oligocene epoch between 24 and 35 Mya, potentially in response to the onset of extremely low CO_2 levels that have characterized the Earth ever since (Ehleringer et al. 1997; Sage 2004; Christin et al. 2011). Because C_4 photosynthesis can operate under much lower ambient CO_2 levels than C_3 , this innovation dramatically expanded the range of atmospheric conditions that would permit land plants to continue functioning on Earth. Since then, the C_4 metabolism has independently emerged in 19 families of plants, with some families displaying multiple originations for a total of at least 62 independent evolutionary lineages (Sage et al. 2011). Given the massive, continuing evolutionary changes that land plants have undergone since their origin ≈ 0.5 Ga, further evolution is plausible over the Gyr timescales considered in this article. One potential evolutionary pathway would be to combine existing carbon concentration mechanisms to ease the physiological stresses imposed by the potentially low CO_2 of the future. In fact, one species of succulent, *Portulaca oleracea*, already displays an integrated C_4 /CAM metabolism, demonstrating the potential viability of stacking carbon concentration mechanisms (Moreno-Villena et al. 2022). Adaptation of land plants to a changing environment could push their extinction to even later dates than predicted here, though the proximity of our maximum biosphere lifetime to predictions for the timing of the onset of the moist or runaway greenhouse suggests that the loss of Earth’s oceans may limit the potential for further evolution of land plants to delay their extinction.

5. CONCLUSION

In this study, we applied a global-mean model of Earth’s climate and carbon cycle, which accounts for the enhancement of silicate weathering by C_3 and C_4 plants, to re-evaluate the lifespan of the complex terrestrial biosphere under a brightening Sun. We show that recent data indicating weakly temperature-dependent silicate weathering (Maher & Chamberlain 2014; Krissansen-Totton & Catling 2017; Graham & Pierrehumbert 2020; Herbert et al. 2022; Brantley et al. 2023) lead to the prediction that biosphere death results from overheating, not CO_2 starvation. These findings suggest that the future lifespan of Earth’s complex biosphere may be nearly twice as long as previously thought. Specifically, if silicate weathering is weakly temperature-dependent and/or strongly CO_2 -dependent, progressive decreases in plant productivity can slow, halt, and even temporarily reverse the expected future decrease in CO_2 as insolation continues to increase. Although this compromises the ability of the silicate weathering feedback to slow the warming of the Earth induced by higher insolation, it can also delay or prevent CO_2 starvation of land plants, allowing the continued existence of a complex land biosphere until the surface temperature becomes too hot. In this regime, contrary to previous results, expected future decreases in CO_2 outgassing and increases in land area would result in longer lifespans for the biosphere by delaying the point when land plants overheat. Importantly, with a revised thermotolerance limit for vascular land plants of 338 K, these results imply that the biotic feedback on weathering may allow complex land life to persist up to the moist or runaway greenhouse transition on Earth (and potentially Earth-like exoplanets). Finally, as discussed in Section 4.1, a longer future lifespan for the complex biosphere may also provide weak statistical evidence that there were fewer “hard steps” in the evolution of intelligent life than previously estimated and that the origin of life was not one of those hard steps.

ACKNOWLEDGMENTS

This research was supported by a University of Chicago International Institute of Research in Paris Faculty Grant. Research was also sponsored by the National Aeronautics and Space Administration (NASA) through a contract with

Oak Ridge Associated Universities (ORAU). The views and conclusions contained in this document are those of the authors and should not be interpreted as representing the official policies, either expressed or implied, of the National Aeronautics and Space Administration (NASA) or the U.S. Government. The U.S. Government is authorized to reproduce and distribute reprints for Government purposes notwithstanding any copyright notation herein. We thank Edwin Kite, Preston Kemeny, and at least 7 anonymous reviewers for providing useful critiques that significantly improved the paper's content and presentation.

Software: Matplotlib (Hunter 2007), Numpy (Harris et al. 2020), Scipy (Jones et al. 2001)

APPENDIX

REFERENCES

- Abbot, D. S. 2016, *The Astrophysical Journal*, 827, 117
- Abbot, D. S., Cowan, N. B., & Ciesla, F. J. 2012, *Astrophysical Journal*, 756, 178
- Aldous, D. J. 2012, *Mathematical Scientist*, 37, 55
- Bahcall, J. N., Pinsonneault, M., & Basu, S. 2001, *The Astrophysical Journal*, 555, 990
- Baum, M., Fu, M., & Bourguet, S. 2022, *Geophysical Research Letters*, e2022GL098843
- Bernacchi, C., Singaas, E., Pimentel, C., Portis Jr, A., & Long, S. P. 2001, *Plant, Cell & Environment*, 24, 253
- Berner, E., Berner, R., & Moulton, K. 2003, *Treatise on geochemistry*, 5, 605
- Berner, R. A. 1992, *Geochimica et Cosmochimica Acta*, 56, 3225
- Björkman, O., Pearcy, R. W., Harrison, A. T., & Mooney, H. 1972, *Science*, 175, 786
- Blunier, T., Bender, M., Barnett, B., & Von Fischer, J. 2012, *Climate of the Past*, 8, 1509
- Bostrom, N. 2013, *Anthropic bias: Observation selection effects in science and philosophy* (Routledge)
- Brantley, S., Shaughnessy, A., Lebedeva, M. I., & Balashov, V. N. 2023, *Science*, 379, 382
- Brown, W. V., & Smith, B. N. 1975, *Bulletin of the Torrey Botanical Club*, 10
- Caldeira, K., & Kasting, J. F. 1992, *Nature*, 360, 721
- Carter, B. 1983, *Philosophical Transactions of the Royal Society of London. Series A, Mathematical and Physical Sciences*, 310, 347
- . 2008, *International Journal of Astrobiology*, 7, 177
- Chen, D.-X., Coughenour, M. B., Knapp, A. K., & Owensby, C. E. 1994, *Ecological Modelling*, 73, 63, doi: [10.1016/0304-3800\(94\)90098-1](https://doi.org/10.1016/0304-3800(94)90098-1)
- Chen, T., Brown, R., & Black, C. 1970, *Weed science*, 18, 399
- Christin, P.-A., Osborne, C. P., Sage, R. F., Arakaki, M., & Edwards, E. J. 2011, *Journal of experimental Botany*, 62, 3171
- Ćirković, M. M., Vukotić, B., & Dragičević, I. 2009, *Astrobiology*, 9, 491
- Clarke, A. 2014, *International Journal of Astrobiology*, 13, 141
- Collatz, G. J., Ribas-Carbo, M., & Berry, J. A. 1992, *Functional Plant Biology*, 19, 519
- Cox, P. M., Huntingford, C., & Harding, R. J. 1998, *Journal of Hydrology*, 212-213, 79, doi: [10.1016/S0022-1694\(98\)00203-0](https://doi.org/10.1016/S0022-1694(98)00203-0)
- Coy, B. P. 2022, PhD thesis, UNIVERSITY OF CHICAGO
- Dahl, T. W., & Arens, S. K. 2020, *Chemical Geology*, 547, 119665
- de Sousa Mello, F., & Friaça, A. C. S. 2020, *International Journal of Astrobiology*, 19, 25
- Deng, K., Yang, S., & Guo, Y. 2022, *Nature communications*, 13, 1
- Dodd, M. S., Papineau, D., Grenne, T., et al. 2017, *Nature*, 543, 60
- Edwards, E. J., & Ogburn, R. M. 2012, *International journal of plant sciences*, 173, 724
- Ehleringer, J. R., Cerling, T. E., & Helliker, B. R. 1997, *Oecologia*, 112, 285
- Farquhar, G. D., von Caemmerer, S. v., & Berry, J. A. 1980, *planta*, 149, 78
- Flambaum, V. V. 2003, *Astrobiology*, 3, 237, doi: [10.1089/153110703769016307](https://doi.org/10.1089/153110703769016307)
- Franck, S., Block, A., Bloh, W. V., et al. 2000, *Tellus B*, 52, 94
- Franck, S., Bounama, C., & Von Bloh, W. 2006, *Biogeosciences*, 3, 85
- Franck, S., Kossacki, K., & Bounama, C. 1999, *Chemical Geology*, 159, 305

- Franck, S., Kossacki, K. J., Von Bloth, W., & Bounama, C. 2002, *Tellus B: Chemical and Physical Meteorology*, 54, 325
- François, L. M., Delire, C., Warnant, P., & Munhoven, G. 1998, *Global and planetary change*, 16, 37
- Galway-Witham, J., & Stringer, C. 2018, *Science*, 360, 1296
- Godsey, S. E., Kirchner, J. W., & Clow, D. W. 2009, *Hydrological Processes*, 23, 1844, doi: [10.1002/hyp.7315](https://doi.org/10.1002/hyp.7315)
- Goldblatt, C., McDonald, V. L., & McCusker, K. E. 2021, *Nature Geoscience*, 1
- Graham, R., & Pierrehumbert, R. 2020, *Astrophysical Journal*, 896
- Hakim, K., Bower, D. J., Tian, M., et al. 2021, *The Planetary Science Journal*, 2, 49
- Hanson, R. 1998a, Unpublished manuscript, September, 23, 168
- . 1998b, preprint available at <http://hanson.gmu.edu/greatfilter.html>
- Hanson, R., Martin, D., McCarter, C., & Paulson, J. 2021, *The Astrophysical Journal*, 922, 182
- Haqq-Misra, J., Kopparapu, R. K., Batalha, N. E., Harman, C. E., & Kasting, J. F. 2016, *The Astrophysical Journal*, 827, 120
- Harris, C. R., Millman, K. J., Van Der Walt, S. J., et al. 2020, *Nature*, 585, 357
- Herbert, T. D., Dalton, C. A., Liu, Z., et al. 2022, *Science*, 377, 116
- Hunter, J. D. 2007, *Computing in science & engineering*, 9, 90
- Ibarra, D. E., Rugenstein, J. K. C., Bachan, A., et al. 2019, *American Journal of Science*, 319, 1
- Jacobs, C. M. J. 1994, Direct impact of atmospheric CO₂ enrichment on regional transpiration (Wageningen University and Research)
- Jones, E., Oliphant, T., Peterson, P., et al. 2001
- Judson, O. P. 2017, *Nature ecology & evolution*, 1, 0138
- Kasting, J. F., Chen, H., & Kopparapu, R. K. 2015, *The Astrophysical Journal Letters*, 813, L3
- Kasting, J. F., Whitmire, D. P., & Reynolds, R. T. 1993, *Icarus*, 101, 108
- Keeley, J. E., & Rundel, P. W. 2003, *International journal of plant sciences*, 164, S55
- Kleidon, A., Fraedrich, K., & Heimann, M. 2000, *Climatic Change*, 44, 471, doi: [10.1023/A:1005559518889](https://doi.org/10.1023/A:1005559518889)
- Krissansen-Totton, J., & Catling, D. C. 2017, *Nature communications*, 8, 1
- Lange, O., Schulze, E. D., Evenari, M., Kappen, L., & Buschbom, U. 1974, *Oecologia*, 17, 97
- Leconte, J., Forget, F., Charnay, B., Wordsworth, R., & Pottier, A. 2013, *Nature*, 504, 268
- Lenton, T. M., & von Bloh, W. 2001, *Geophysical research letters*, 28, 1715
- Lin, Y.-S., Medlyn, B. E., & Ellsworth, D. S. 2012, *Tree physiology*, 32, 219
- Lingam, M., & Loeb, A. 2019, *International Journal of Astrobiology*, 18, 527
- Lovelock, J. E., & Whitfield, M. 1982, *Nature*, 296, 561
- Maher, K., & Chamberlain, C. 2014, *Science*, 343, 1502
- Manabe, S., Wetherald, R. T., Milly, P. C. D., Delworth, T. L., & Stouffer, R. J. 2004, *Climatic Change*, 64, 59, doi: [10.1023/B:CLIM.0000024674.37725.ca](https://doi.org/10.1023/B:CLIM.0000024674.37725.ca)
- Márquez, L. M., Redman, R. S., Rodriguez, R. J., & Roossinck, M. J. 2007, *science*, 315, 513
- Medlyn, B. E., Duursma, R. A., Eamus, D., et al. 2011, *Global Change Biology*, 17, 2134
- . 2012, *Global Change Biology*, 18, 3476
- Mello, F. d. S., & Friaça, A. C. S. 2023, *International Journal of Astrobiology*, 1, doi: [10.1017/S1473550423000083](https://doi.org/10.1017/S1473550423000083)
- Miller, S. R., McGuirl, M. A., & Carvey, D. 2013, *Molecular biology and evolution*, 30, 752
- Moreno-Villena, J. J., Zhou, H., Gilman, I. S., et al. 2022, *Science Advances*, 8, eabn2349
- Moulton, K. L., & Berner, R. A. 1998, *Geology*, 26, 895
- Moulton, K. L., West, J., & Berner, R. A. 2000, *American Journal of Science*, 300, 539
- Nobel, P. S. 2020, in *Physicochemical and Environmental Plant Physiology* (Elsevier), 409–488, doi: [10.1016/B978-0-12-819146-0.00008-0](https://doi.org/10.1016/B978-0-12-819146-0.00008-0)
- O'Malley-James, J. T., Greaves, J. S., Raven, J. A., & Cockell, C. S. 2013, *International Journal of Astrobiology*, 12, 99, doi: [10.1017/S147355041200047X](https://doi.org/10.1017/S147355041200047X)
- Ozaki, K., & Reinhard, C. T. 2021, *Nature Geoscience*, 14, 138
- Palandri, J. L., & Kharaka, Y. K. 2004, A compilation of rate parameters of water-mineral interaction kinetics for application to geochemical modeling, Tech. rep.
- Pearce, B. K., Tupper, A. S., Pudritz, R. E., & Higgs, P. G. 2018, *Astrobiology*, 18, 343
- Pennisi, E. 2003, Fungi shield new host plants from heat and drought, American Association for the Advancement of Science
- Perkins, J. 2021, *Field Studies in Ecology*, 3
- Popp, M., Schmidt, H., & Marotzke, J. 2016, *Nature Communications*, 7, 10627
- Prado, K., Xue, B., Johnson, J. E., et al. 2023, *bioRxiv*, 2023

- Raven, J. A., Cockell, C. S., & De La Rocha, C. L. 2008, *Philosophical Transactions of the Royal Society B: Biological Sciences*, 363, 2641, doi: [10.1098/rstb.2008.0020](https://doi.org/10.1098/rstb.2008.0020)
- Redman, R. S., Sheehan, K. B., Stout, R. G., Rodriguez, R. J., & Henson, J. M. 2002, *Science*, 298, 1581
- Rogers, A., & Humphries, S. W. 2000, *Global Change Biology*, 6, 1005, doi: [10.1046/j.1365-2486.2000.00375.x](https://doi.org/10.1046/j.1365-2486.2000.00375.x)
- Rushby, A. J., Johnson, M., Mills, B. J., Watson, A. J., & Claire, M. W. 2018, *Astrobiology*, 18, 469
- Sage, R. F. 2004, *New Phytologist*, 161, 341, doi: [10.1111/j.1469-8137.2004.00974.x](https://doi.org/10.1111/j.1469-8137.2004.00974.x)
- Sage, R. F., Christin, P.-A., & Edwards, E. J. 2011, *Journal of experimental botany*, 62, 3155
- Salvucci, M. E., & Crafts-Brandner, S. J. 2004, *Plant physiology*, 134, 1460
- Salvucci, M. E., Osteryoung, K. W., Crafts-Brandner, S. J., & Vierling, E. 2001, *Plant physiology*, 127, 1053
- Scafaro, A. P., Bautsoens, N., Den Boer, B., Van Rie, J., & Gallé, A. 2019, *Plant Physiology*, 181, 43
- Scafaro, A. P., Posch, B. C., Evans, J. R., Farquhar, G. D., & Atkin, O. K. 2023, *Nature Communications*, 14, 2820
- Schwartzman, D. W. 2017, *AIMS Geosciences*, 3, 216, doi: [10.3934/geosci.2017.2.216](https://doi.org/10.3934/geosci.2017.2.216)
- Seager, S., Turner, E., Schafer, J., & Ford, E. 2005, *Astrobiology*, 5, 372
- Shivhare, D., & Mueller-Cajar, O. 2017, *Plant Physiology*, 174, 1505
- Snyder-Beattie, A. E., & Bonsall, M. B. 2022, *Proceedings of the Royal Society B*, 289, 20212711
- Snyder-Beattie, A. E., Sandberg, A., Drexler, K. E., & Bonsall, M. B. 2021, *Astrobiology*, 21, 265
- Stephens, G. L., O'Brien, D., Webster, P. J., et al. 2015, *Reviews of geophysics*, 53, 141
- Tansey, M. R., & Brock, T. D. 1972, *Proceedings of the National Academy of Sciences*, 69, 2426
- Taylor, L., Banwart, S., Leake, J., & Beerling, D. J. 2011, *American Journal of Science*, 311, 369, doi: [10.2475/05.2011.01](https://doi.org/10.2475/05.2011.01)
- Taylor, L., Leake, J., Quirk, J., et al. 2009, *Geobiology*, 7, 171
- Valley, J. W., Peck, W. H., King, E. M., & Wilde, S. A. 2002, *Geology*, 30, 351
- Volk, T. 1987, in *American Journal of Science*, 763–779
- Von Bloh, W., Franck, S., Bounama, C., & Schellnhuber, H.-J. 2003, *Geomicrobiology Journal*, 20, 501
- Walker, J. C. G., Hays, P. B., & Kasting, J. F. 1981, *Journal of Geophysical Research*, 86, 9776
- Waltham, D. 2017, *Astrobiology*, 17, 61
- Watson, A. 2004, in *Scientists debate Gaia: the next century* (MIT Press), 201–208
- Watson, A. J. 2008, *Astrobiology*, 8, 175
- Winnick, M. J., & Maher, K. 2018, *Earth and Planetary Science Letters*, 485, 111
- Wolf, E., Haqq-Misra, J., & Toon, O. 2018, *Journal of Geophysical Research: Atmospheres*, 123, 11
- Wolf, E., & Toon, O. 2014, *Geophysical Research Letters*, 41, 167
- . 2015, *Journal of Geophysical Research*, 120, 5775
- Wong, S., Cowan, I., & Farquhar, G. 1979, *Nature*, 282, 424
- Yan, M., Yang, J., Zhang, Y., & Huang, H. 2022, *Geophysical Research Letters*, 49, e2022GL100152, doi: [10.1029/2022GL100152](https://doi.org/10.1029/2022GL100152)
- Yang, J.-W., Brandon, M., Landais, A., et al. 2022, *Science*, 375, 1145